Supporting Information for "Approximating 3D Models of Planetary Evolution in 2D: A Comparison of Different Geometries"

Aymeric Fleury[1], Ana-Catalina Plesa[1], Christian Hüttig[1], Doris Breuer[1]

[1]Institute of Planetary Research, German Aerospace Center (DLR), Berlin, Germany

Contents of this file

Additional Supporting Information (Files uploaded separately)

Introduction

In Section S1 we present the scaling factors used in this study, as listed in Table S1. Section S2 displays in Table S2 all the parameters used to create the grids employed in this study for the thermal convection model GAIA. Section S3 details the differences between the cylindrical and the spherical annulus geometries used in our thermal convection code GAIA. Section S4 provides a short comparison between the study from *Hernlund and Tackley* (2008) and this study for isoviscous stead-state cases. Section S5 presents how the relative error is calculated. In Section S6 we give briefly the equations used for internal heating and the decay of heat producing elements in our model. In Sections S7 and S8 we list the tables displaying all the present-day values of the investigated output quantities for the thermal evolution scenario in an homogeneous setup (S7) and in a setup with a 50 km crust (S8); these data are available as CSV files provided at . Section S9 presents the temperature profiles at present day and at 1 Gyr into the evolution for each thermal evolution scenario with a 50 km crust. Section S10 shows the calculation of the stagnant lid thickness for the thermal evolution models. Section S11 displays the calculation of the partial melting in the mantle, as a post processing step for the thermal evolution models. Section S12 gives the formulation to calculate the thickness of the mechanical lithosphere as a post processing step. In the Section S13, three different comparisons of stagnant lid simulations (see Section 4), are displayed as slices for both the 3D spherical shell and the 2D spherical annulus geometry, with the 3D on the left and the 2D geometry on the right.

S1 Scaling table

The conservation equations used to model mantle convection are expressed in non-dimensional form. The non-dimensionalisation is obtained by multiplying the parameters by a well-suited scaling factor. Parameters with a star represent the non-dimensional ones and are calculated as follows:

Quantity	Non dimensional
Temperature	$T^* = \frac{T-T_0}{\Delta T}$
Length	$x^* = \frac{x}{D}$
Time	$t^* = \frac{\kappa_0}{D^2}t$
Velocity	$u^* = \frac{uD}{\kappa_0}$
Pressure	$P^* = \frac{PD^2}{\eta_0 \kappa_0}$
Stress	$\sigma^* = \sigma\frac{D^2}{\eta_0 \kappa_0}$
Density	$\rho^* = \frac{\rho}{\rho_0}$
Thermal expansivity	$\alpha^* = \frac{\alpha}{\alpha_0}$
Heat production rate	$H^* = \frac{HD^2}{\kappa_0 cp \Delta T}$
Viscosity	$\eta^* = \frac{\eta}{\eta_0}$
Activation energy	$E^* = \frac{E}{\Delta TR}$
Activation volume	$V^* = \frac{V\rho_0 Dg}{\Delta TR}$

Table S1: Table of the non dimensional values used in the study

In the remainder of this study, all the non-dimensional parameters are used without the star for better readability.

Setup	Geometry	Aspect ratio	Radial resolution	Lateral resolution	Total points	Rayleigh number
	$2-D$	0.2	48 shells	227 p.per.shell	11350	$10^4-10^5-10^6$
	$2-D$	0.4	48 shells	352 p.per.shell	17600	$10^4-10^5-10^6$
	$2-D$	0.6	48 shells	604 p.per.shell	30200	$10^4-10^5-10^6$
	$2-D$	0.8	48 shells	1358 p.per.shell	67900	$10^4-10^5-10^6$
	$2-D$	0.2	120 shells	556 p.per.shell	69052	10^7-10^8
	$2-D$	0.4	120 shells	880 p.per.shell	107360	10^7-10^8
	$2-D$	0.6	120 shells	1508 p.per.shell	183976	10^7-10^8
Isoviscous	$2-D$	0.8	120 shells	3393 p.per.shell	413946	10^7-10^8
	$3-D$	0.2	48 shells	40962 p.per.shell	2048100	$10^4-10^5-10^6$
	$3-D$	0.4	48 shells	40962 p.per.shell	2048100	$10^4-10^5-10^6$
	$3-D$	0.6	48 shells	40962 p.per.shell	2048100	$10^4-10^5-10^6$
	$3-D$	0.8	48 shells	40962 p.per.shell	2048100	$10^4-10^5-10^6$
	$3-D$	0.2	70 shells	40962 p.per.shell	2949264	10^7-10^8
	$3-D$	0.4	70 shells	40962 p.per.shell	2949264	10^7-10^8
	$3-D$	0.6	70 shells	40962 p.per.shell	2949264	10^7-10^8
	$3-D$	0.8	70 shells	40962 p.per.shell	2949264	10^7-10^8
	$2-D$	0.2	100 shells	472 p.per.shell	48144	$Ra = 5 \times 10^6; Ra_Q = 5 \times 10^7$
	$2-D$	0.5	100 shells	943 p.per.shell	96186	–
T-dependent	$2-D$	0.8	100 shells	2828 p.per.shell	288456	–
	$3-D$	0.2	70 shells	40962 p.per.shell	2949264	–
	$3-D$	0.5	70 shells	40962 p.per.shell	2949264	–
	$3-D$	0.8	70 shells	40962 p.per.shell	2949264	–
	$2-D$	Mars $\rightarrow$ 0.544117	155 shells	1 650 p.per.shell	259050	$Ra = 2.14 \times 10^6; Ra_Q = 5.91 \times 10^7$
	$3-D$	-	70 shells	40962 p.per.shell	2949264	–
Thermal	$2-D$	Moon $\rightarrow$ 0.224137	135 shells	670 p.per.shell	91790	$Ra = 5.35 \times 10^5; Ra_Q = 8.70 \times 10^6$
evolution	$3-D$	-	64 shells	40962 p.per.shell	2703492	–
	$2-D$	Mercury $\rightarrow$ 0.827868	84 shells	2803 p.per.shell	241058	$Ra = 3.49 \times 10^4; Ra_Q = 8.00 \times 10^4$
	$3-D$	-	46 shells	40962 p.per.shell	1884252	–

Table S2: Grid parameters for each simulation in this study. For each grid, the number of shells displayed is the number of layers in the "active" part of the grid, meaning that it does not account for the two ghost layers at the base and at the top of the grid, which are used to set the boundary conditions.

S2 Grid parameters

This table provides all the grid parameters used in this study for the steady state simulations as well as the thermal evolution models.
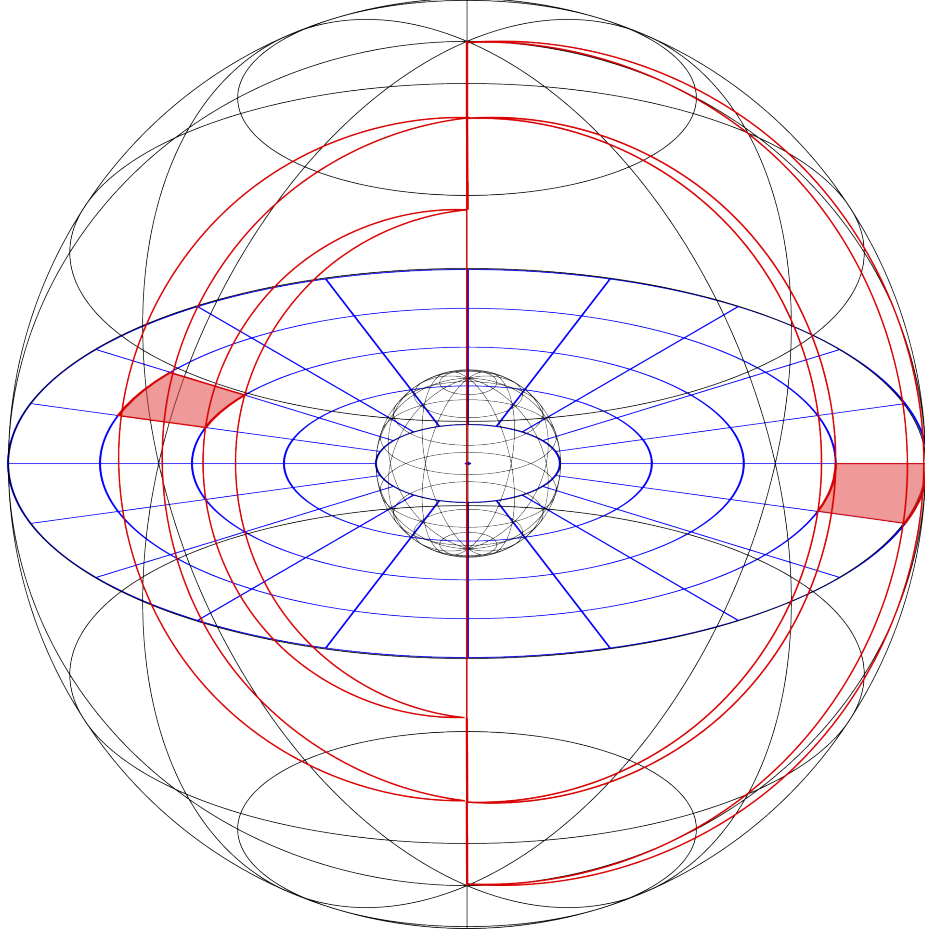
Figure S1: Representation of the elementary volumes of the cylinder in blue and of the spherical annulus in red. In a regular two dimensional representation of the spherical annulus grid, we only see the area of the elementary volume bisected by the equatorial plane (red filled areas).

S3 Spherical annulus geometry

The principal difference between the 2D spherical annulus and the 2D cylindrical geometry lies in the formulation of the areas and volumes for each grid. The cylindrical geometry will have a purely 2D formulation of its areas and volume whereas the spherical annulus use the same formulation as a 3D spherical shell. The effective degree of curvature for each cell goes then from 1 in the case of the cylinder to 2 in the case of the spherical annulus. For the mathematical formulation of the grid geometry, we refer to *Hernlund and Tackley*, 2008

S4 Comparison to results of Hernlund and Tackley 2008

This table presents the comparison between the study from *Hernlund and Tackley*, 2008 and this study for isoviscous steady state cases considering basal heating and internal heating, respectively, with Rayleigh numbers between $Ra = 10^4$ to $Ra = 10^5$. For the radius an Earth-like value is used (f= 0.55) for the 3D spherical shell and the annulus, while the scaled cylinder uses f= 0.3025. The values are averaged over the last 20% of the simulations.

Ra $= 10^4$	Geometry	Bottom heated		
		3D	Spherical annulus	Scaled cylindrical
Hernlund & Tackley 2008	v_{rms}	42.3	37.7	35.6
	v_{rms} peak-peak	0	0	0
	<Nu>	3.85	4.18	3.99
	<Nu> peak-peak	steady	steady	steady
This study	v_{rms}	42.1	43.1	37.3
	v_{rms} peak-peak	0	0	0
	<Nu>	3.84	4.12	4.08
	<Nu> peak-peak	steady	steady	steady
Ra $= 10^5$				
Hernlund & Tackley 2008	v_{rms}	160	160	165
	v_{rms} peak-peak	11	14	90
	<Nu>	7.27	7.39	6.2
	<Nu> peak-peak	0.5	0.3	2.1
This study	v_{rms}	163.9	160.0	158.1
	v_{rms} peak-peak	1	10	0
	<Nu>	6.62	7.16	7.75
	<Nu> peak-peak	0.03	0.4	0.2
		Internal heated		
Ra $= 10^4$	$Ra_Q = 3.4 \times 10^4$			
Hernlund & Tackley 2008	v_{rms}	23.3	23.5	22.8
	v_{rms} peak-peak	0	0	0
	<T>	0.311	0.308	0.319
This study	v_{rms}	22.6	23.3	21.4
	v_{rms} peak-peak	0	0	0
	<T>	0.311	0.312	0.334
Ra $= 10^5$	$Ra_Q = 6.6 \times 10^5$			
Hernlund & Tackley 2008	v_{rms}	60.5	78.5	77.0
	v_{rms} peak-peak	7	36	75
	<T>	0.322	0.349	0.384
This study	v_{rms}	76.7	84.6	79.7
	v_{rms} peak-peak	2.2	9	10.5
	<T>	0.337	0.3443	0.387

Table S3: Comparison of the spherical annulus used in this study and the study of *Hernlund and Tackley*, 2008. The top part of the table are the results from *Hernlund and Tackley*, 2008 and the bottom part of the table present the results from this study. The values displayed are the root mean square velocity (v_{rms}), mean temperature (<T>), and Nusselt numbers (Nu), which are computed once a statistical steady state is attained.

S5 Error computation

The error presented in the main manuscript to illustrate the difference between 2D and 3D geometries was computed as follows:

$$Error = -\frac{(3D_{value} - 2D_{value})}{max(3D_{value}; 2D_{value})} \times 100 \tag{S1}$$

The absolute error for the thermal evolution simulations on the other hand is calculated as:

$$Error = 2D_{dimensionalvalue} - 3D_{dimensionalvalue} \tag{S2}$$

in order to determine whether a 2D geometry over or under-estimates the 3D geometry results.

S6 Internal heating and heat producing elements decay

In our thermal evolution scenarii, we also take into account the decay of the heat producing elements, here being the Ur^{238}, Ur^{235}, Th^{232} and the K^{40}, thus giving us the heat production rate which is determined from present day amounts of heat sources and is given by equation 28 from *Breuer* (2009).

S7 Table of results for the thermal evolution simulations without crust

This table gives all the present-day values in a dimensional form for the thermal evolution simulations without crust.

Planet	Parameter (Unit)	3D sph. shell	2D sph. annulus	2D scaled cylinder	2D cylinder
Mars	T_{mean} (K)	1697.1	1713.9	1752.8	1846.3
	T_{CMB} (K)	2146.8	2150.2	2189.3	2171.1
	v_{rms} (cm/yr)	0.767	1.04	1.05	1.32
	q_{top} (mW/m^2)	21.68	22.95	24.10	27.12
	q_{bot} (mW/m^2)	2.10	2.12	1.91	1.07
	D_{lid} (km)	302.5	297.1	281.52	247.7
Moon	T_{mean} (K)	1367.6	1372.7	1552.6	1661.8
	T_{CMB} (K)	2379.7	2403.6	2473.2	2287.9
	v_{rms} (cm/yr)	0.216	0.374	0.527	0.472
	q_{top} (mW/m^2)	14.533	14.47	17.05	18.15
	q_{bot} (mW/m^2)	0.959	0.910	0.723	-3.35
	D_{lid} (km)	415.1	427.5	377.2	358.5
Mercury	T_{mean} (K)	1049.3	1048.0	1069.8	1155.6
	T_{CMB} (K)	1689.0	1685.1	1715.9	1829.2
	v_{rms} (cm/yr)	5.7E-4	3.1E-07	5.9E-07	7.7E-05
	q_{top} (mW/m^2)	12.85	12.83	13.56	15.29
	q_{bot} (mW/m^2)	10.20	10.15	10.10	10.74
	D_{lid} (km)	294.9	252.9	248.2	244.0

Table S4: Output quantities at present day for various geometries and planets in an homogeneous set.

S8 Table of results for the thermal evolution simulations with a 50 km crust

This table gives all the present-day values for the thermal evolution simulations with crust.

Planet	Parameter (Unit)	3-D sph. shell	2-D sph. annulus	2-D scaled cylinder	2-D cylinder
	T_{mean} (K)	1700.4	1741.8	1774.4	1846.1
	T_{CMB} (K)	2123.4	2147.5	2169.2	2109.2
Mars	v_{rms} (cm/yr)	0.73	1.00	1.03	0.92
	q_{top} (mW/m^2)	21.78	23.22	24.15	26.53
	q_{bot} (mW/m^2)	1.65	1.29	1.19	-1.68
	D_{lid} (km)	277.00	259.80	254.61	233.17
	T_{mean} (K)	1456.9	1481.6	1658.1	1756.8
	T_{CMB} (K)	2404.7	2435.1	2504.9	2296.6
Moon	v_{rms} (cm/yr)	0.24	0.35	0.68	0.50
	q_{top} (mW/m^2)	14.63	14.53	16.95	17.93
	q_{bot} (mW/m^2)	0.38	0.30	0.22	-1.86
	D_{lid} (km)	368.2	370.9	327.3	305.7
	T_{mean} (K)	1049.3	1048.7	1070.5	1155.5
	T_{CMB} (K)	1689.0	1686.9	1716.7	1830.1
Mercury	v_{rms} (cm/yr)	5.7E-04	5.1E-05	6.2E-07	1.6E-3
	q_{top} (mW/m^2)	12.8	12.8	13.6	15.2
	q_{bot} (mW/m^2)	10.2	10.1	10.8	10.1
	D_{lid} (km)	294.8	292.7	275.7	296.5

Table S5: Output quantities at present day for each planet in various geometries for the thermal evolution simulation with a 50km crust.

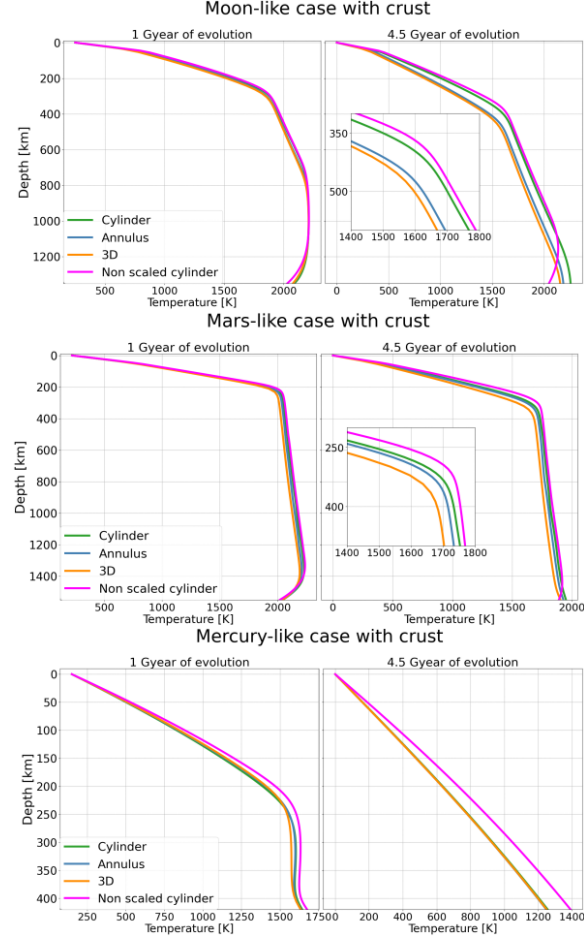All the present day output quantities are available in the online CSV files of this study.

Figure S2: Profiles of temperature throughout the entire mantle for the Moon, Mars and Mercury. The profiles are shown at 1 billion years into the evolution and at present day. Every geometry studied is represented here; in the case of Mercury, only the simulations with a reference viscosity $\eta_{ref} = 10^{21}$ Pa s are shown.

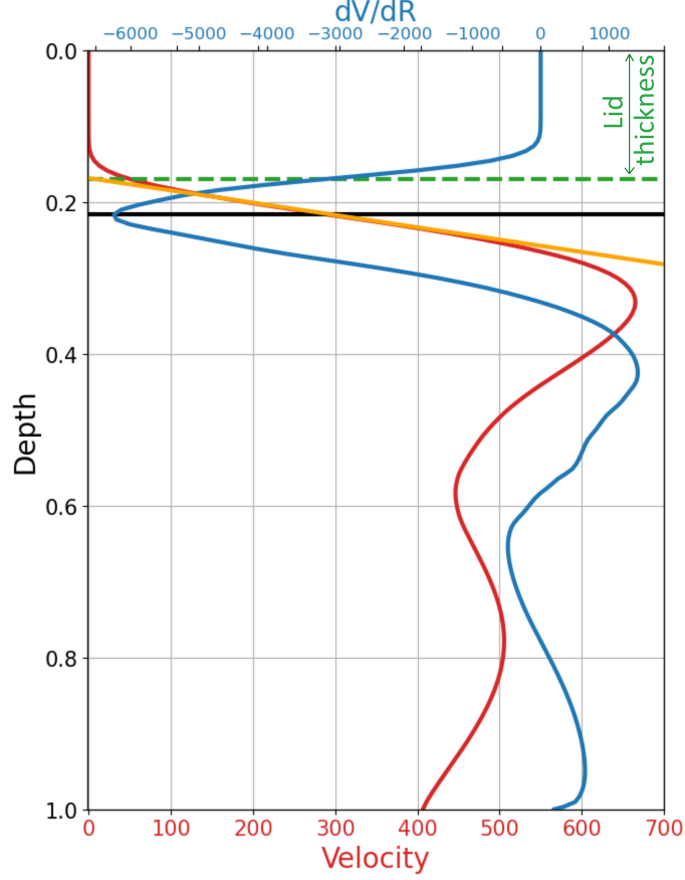## S9 Temperature profiles for thermal evolution simulations

Figure S3: Calculation of the stagnant lid thickness adapted from the work of *Hüttig and Breuer* (2011). The thickness is determined by finding the depth where the derivative of the averaged velocity profile $\frac{dV}{dR}$ is the highest and intercepting it with the y axis. The red line is the averaged velocity profile in the domain, the blue line is the derivative of the velocity profile, the green dashed line is the depth of the stagnant lid, and the black line is the depth of the absolute value of the velocity derivative is the highest. All units are non dimensional.

S10 Stagnant lid calculation

In the calculation of the stagnant lid we use two different methods to determine its thickness. The first is from the work of *Hüttig and Breuer* (2011) and is illustrated by the Figure S3 The calculation of the stagnant lid becomes difficult with the velocity gradient method (*Hüttig and Breuer*, 2011) when the veolocity are too low. Therefore a second method, relying on the Peclet criterion is used in the case of Mercury when it falls into a quasi conductive state. The determination of the stagnant lid with a Peclet criterion, is determined with a threshold, that we set here as 5% of the averaged v_{rms} at the studied time step. The thickness is then the depth at which the v_{rms} profile becomes smaller than our threshold (or Peclet criterion).
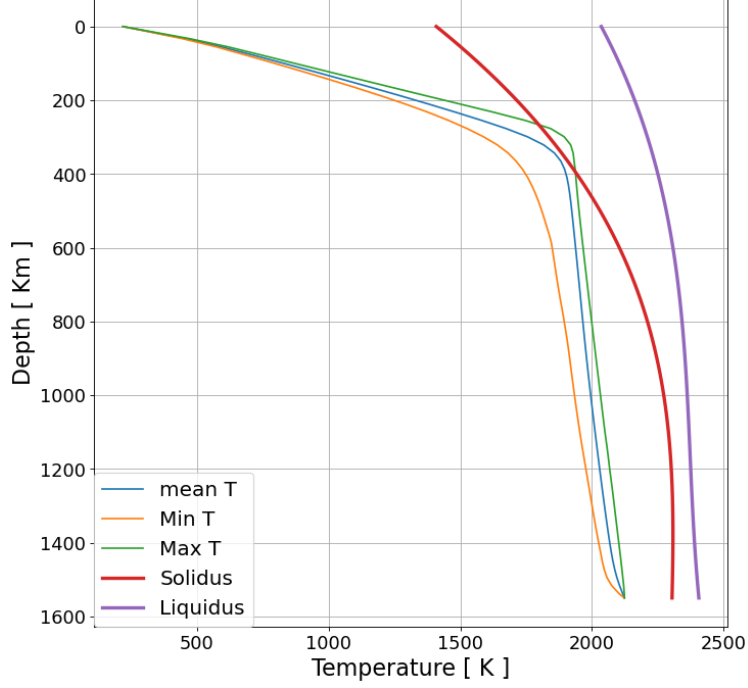
Figure S4: Melting curves from *Takahashi* (1990) and the minimum, mean and maximum temperature profile for a present-day Mars-like case.

S11 Partial melting calculation

We compute the averaged fraction of molten mantle at every time-step during the thermal evolution of the planet as a post processing step. It is used here as a simple comparison between the geometries. We use the melting curves from *Takahashi* (1990), as seen on Figure S2. However a cutoff is imposed at a depth of 7 GPa in the case of Mars. To calculate the volumetrically averaged degree of melting, we use eq 20. from *Morschhauser et al.* (2011) which is as following :

$$m_a = \frac{1}{V_a} \int_{V_a} \frac{T(r) - T_{sol}(r)}{T_{liq}(r) - T_{sol}(r)} \, dV, \tag{S3}$$

with V_a being the volume of the meltzone, T_{sol} the temperature of the solidus, T_{liq} the temperature of the liquidus, and $T(r)$ the calculated mantle temperature profile. We then compute the total volume of melted mantle and compare it with the total mantle volume.

14

Parameter	Crust	Mantle
$\dot{\epsilon}$ (s^{-1})	10^{-17}	10^{-17}
Q (kJ mol^{-1})	488	540
B (Pa^{-n} s^{-1})	1.1×10^{-26}	2.4×10^{-16}
n (-)	4.7	3.5
σ_y (MPa)	15	15

Table S6: Rheological parameters used in the equation S6, as appropriate for dry diabase crust and dry olivine mantle, for more information see *Plesa et al.* (2016), *Grott and Breuer* (2008).

S12 Mechanical thickness calculation

In this study we calculate the mechanical thickness, by using the strength envelope formalism *McNutt* (1984) for a structure comprised of a mantle layer and a crust layer. This mechanical thickness of the lithosphere represents the depth at which the plate looses its mechanical strength due to ductile flow *Grott et al.* (2007). This depth, or temperature equivalent is then calculated as following :

$$T_e = \frac{E}{R} \left[log \left(\frac{\sigma_B^n A}{\dot{\epsilon}} \right) \right]^{-1}, \tag{S4}$$

in which E, A and n are rheological parameter listed in Table S6, R is the gas constant, σ_B the bounding stress, and $\dot{\epsilon}$ being the strain rate. The total elastic thickness of this system depends then on whether the two layers act as a single elastic layer or are separated by an incompetent layer of crust. If the layers are separated, the elastic thickness D_e is then calculated as:

$$D_e = (D_{e,m}^3 + D_{e,c}^3)^{\frac{1}{3}}, \tag{S5}$$

where $D_{e,m}$ and $D_{e,c}$ are the thicknesses of the elastic parts of crust and mantle, respectively *Burov and Diament* (1995). However, if $D_{e,c}$ is greater or equals the local crustal thickness, then no layer of incompetent crust exists between the crust and the mantle and the effective elastic thickness is given by the sum of the two elastic layers:

$$D_e = D_{e,m} + D_{e,c} \tag{S6}$$

The decoupling of the system will strongly reduce the total elastic thickness as seen in eq. S5 and will mostly happen in regions with a thick crust. In the case of our simulations with a laterally homogeneous crust thickness we don't have any zone with a local thicker crust. To compute the local elastic thickness, a strain rate $\dot{\epsilon}$ profiles of 10^{-17} s^{-1} is used. The parameters used for this calculation are available in the Table S5.
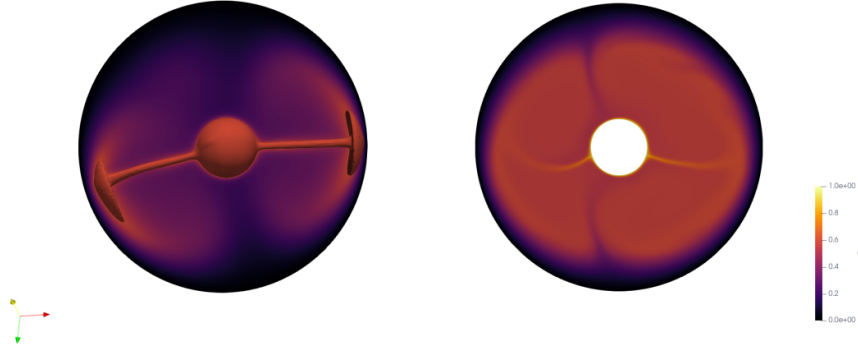
Figure S5: Temperature slices in a temperature-dependent viscosity case with purely basal heating, left is 3D spherical shell and right is 2D spherical annulus. Two plumes are present in both geometries, however the distribution of the temperature is much more diffuse in the case of the annulus, as seen in *Guerrero et al.* (2018).

S13 Slices comparison 3D-2D in stagnant lid simulations

The plots presented here show special cases of comparison between 3D and 2D spherical annulus for different heating mode in temperature-dependent viscosity setups.
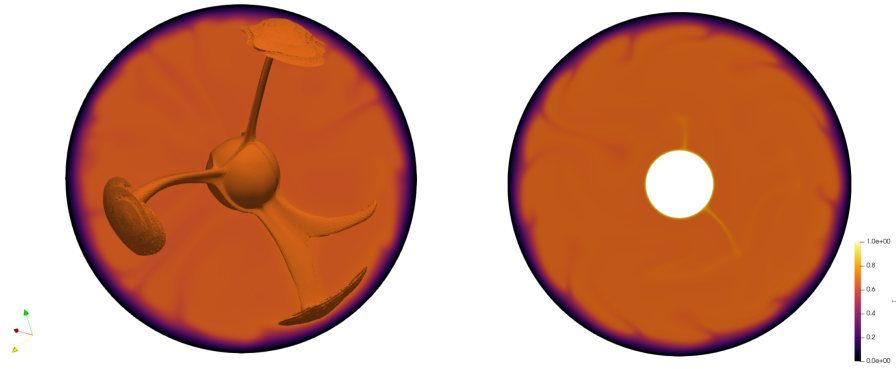
Figure S6: Temperature slices in a temperature-dependent viscosity case with basal and internal heating. We note the disappearance of the error of the temperature distribution seen in Figure S1 by the addition of internal heating.
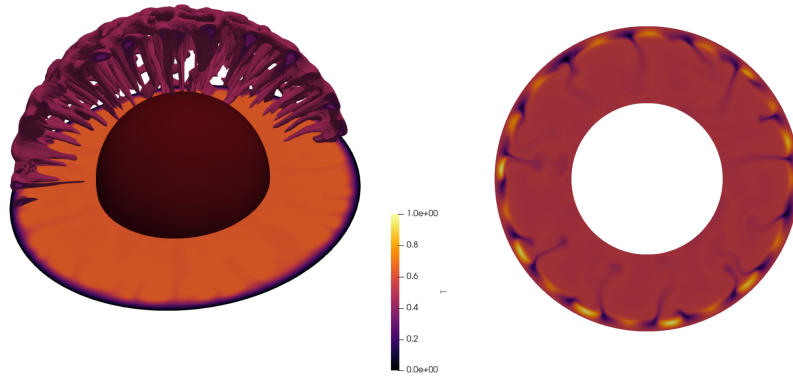

Figure S7: Temperature slices in a temperature-dependent viscosity case with purely internal heating. The amount of downwellings in a slice for the 3D case is far larger than what can be seen for the 2D spherical annulus (2D).

Supplementary datasets

The following datasets are available upon request on Zenodo :

https://doi.org/10.5281/zenodo.8047757

Datasets concerning isoviscous simulations

Tables containing the time averaged (on the last 10% of the run) values for all the outputs and geometry studied. There is one table per Ra number with a given heating mode. In total there are 15 tables for each scenarios (i.e., three different heating modes and five different Ra numbers).

Datasets concerning temperature dependent simulations

Tables containing the time averaged (on the last 10% of the run) values for all the outputs and geometry studied for temperature dependent viscosity simulations. Only one Ra is investigated. In total three tables, for three heating modes.

Datasets concerning thermal evolution simulations with and without crust

Tables containing dimensional present day values of all the investigated outputs for different geometries and planet scenarios for cases with and without crust. In total six tables, for three planets.

References

Breuer, D., 4.2.3.4 dynamics and thermal evolution: Datasheet from landolt-börnstein - group vi astronomy and astrophysics · volume 4b: "solar system" in springermaterials (https://doi.org/10.1007/978-3-540-88055-4_19), doi:10.1007/978-3-540-88055-4_19, copyright 2009 Springer-Verlag Berlin Heidelberg, 2009.

Burov, E.-B., and M. Diament, The effective elastic thickness (Te) of continental lithosphere: What does it really mean?, *J. Geophys. Res.*, *100*, 3905–3927, 1995.

Grott, M., and D. Breuer, The evolution of the Martian elastic lithosphere and implications for crustal and mantle rheology, *Icarus*, *193*, 503–515, doi:10.1016/j.icarus.2007.08.015, 2008.

Grott, M., J. Helbert, and R. Nadalini, Thermal structure of Martian soil and the measurability of the planetary heat flow, *J. Geophys. Res.*, *112*, E09,004, doi:10.1029/2007JE002905, 2007.

Guerrero, J. M., J. P. Lowman, F. Deschamps, and P. J. Tackley, The influence of curvature on convection in a temperature-dependent viscosity fluid: Implications for the 2-d and 3-d modeling of moons, *Journal of Geophysical Research: Planets*, *123*(7), 1863–1880, doi:https://doi.org/10.1029/2017JE005497, 2018.

Hernlund, J. W., and P. J. Tackley, Modeling mantle convection in the spherical annulus, *Physics of the Earth and Planetary Interios*, *171*, 48–54, doi:10.1016/j.pepi.2008.07.037, 2008.

Hüttig, C., and D. Breuer, Regime classification and planform scaling for internally heated mantle convection, *Physics of the Earth and Planetary Interios*, *186(3-4)*, 111–124, 2011.

McNutt, M. K., Lithospheric flexure and thermal anomalies, *J. Geophys. Res.: Solid Earth*, *89*(B13), 11,180–11,194, doi:10.1029/JB089iB13p11180, 1984.

Morschhauser, A., M. Grott, and D. Breuer, Crustal recycling, mantle dehydration, and the thermal evolution of Mars, *Icarus*, *212*, 541–558, doi:10.1016/j.icarus.2010.12.028, 2011.

Plesa, A.-C., M. Grott, N. Tosi, D. Breuer, T. Spohn, and M. A. Wieczorek, How large are present-day heat flux variations across the surface of Mars?, *J. Geophys. Res.*, *121*(12), 2386–2403, doi:10.1002/2016JE005126, 2016.

Takahashi, E., Speculations on the archean mantle: Missing link between komatiite and depleted garnet peridotite, *J. Geophys. Res.*, *95(B10)*, 15,941–15,954, 1990.